As(III) Sequestration by Iron Nanoparticles: Study of Solid-Phase Redox Transformations with X-ray Photoelectron Spectroscopy

ARTICLE *in* THE JOURNAL OF PHYSICAL CHEMISTRY C · FEBRUARY 2012

Impact Factor: 4.77 · DOI: 10.1021/jp208600n

4 AUTHORS, INCLUDING:

Weile Yan
Texas Tech University
16 PUBLICATIONS **465** CITATIONS
SEE PROFILE

Bruce Koel
Princeton University
296 PUBLICATIONS **9,075** CITATIONS
SEE PROFILE

THE JOURNAL OF PHYSICAL CHEMISTRY C

Article

pubs.acs.org/JPCC

As(III) Sequestration by Iron Nanoparticles: Study of Solid-Phase Redox Transformations with X-ray Photoelectron Spectroscopy

Weile Yan,[†,⊥] Mauricio A. V. Ramos,[‡] Bruce E. Koel,[‡,§] and Wei-xian Zhang*[,†,∥]

[†]Center for Advanced Materials and Nanotechnology Department of Civil and Environmental Engineering and [‡]Department of Chemistry, Lehigh University, Bethlehem, Pennsylvania 18015, United States

[§]Department of Chemical and Biological Engineering, Princeton University, Princeton, New Jersey 08544, United States

[∥]State Key Laboratory of Pollution Control and Resources Reuse, College of Environmental Science and Engineering, Tongji University, Shanghai, P. R. China 20092

Supporting Information

ABSTRACT: Nanoscale zerovalent iron (nZVI) has shown a high efficacy for removing arsenite (As(III)), a groundwater contaminant of great concern, yet the chemical transformations of As(III) enabled by nZVI during the sequestration process are not well understood. Using high-resolution X-ray photoelectron spectroscopy (HR-XPS), arsenic in multiple valence states was observed for nZVI particles reacted with aqueous As(III), which establishes that nZVI is capable of inducing As(III) oxidation and reduction, a unique attribute imparted by the core−shell nature of nZVI particles. Time-dependent analysis shows that As(III) oxidation was a facile and reversible reaction taking place at the surface of the iron oxide shell, whereas As(III) reduction occurred at a slower rate and led to gradual diffusion and accumulation of reduced arsenic at a subsurface layer near the Fe(0) core. Long-term (146 days) exposure of the arsenic-laden nZVI in an aqueous environment caused progressive depletion of the Fe(0) cores; however, arsenic was retained in the native oxide shell without leaching into the aqueous phase. The speciation of arsenic in the nanoparticles is strongly dependent on the loading of nZVI. While a large proportion of the arsenic was bound in a reduced state in the presence of ample nZVI, nZVI-limiting conditions resulted in rapid depletion of the Fe(0) cores and enclosure of arsenic within the oxide formation. These results show that the mechanism of nZVI-mediated arsenite removal is substantially different from that of conventional iron oxide-based adsorbents. Encapsulation of arsenic into the bulk of the solid phase suggests nZVI a potentially more capacious and robust sequestration agent for arsenic abatement.

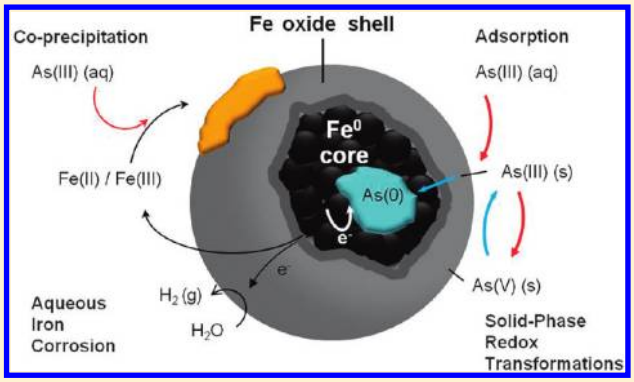

INTRODUCTION

High levels of arsenic in groundwater pose a serious health threat to millions of people around the world.[1,2] The situation is of particular concern in rural areas of developing countries such as Bangladesh, India, Vietnam, and Cambodia, where there is no centralized water treatment facility and the contaminated groundwater is heavily utilized for drinking and irrigation of food crops.[3,4] Severe health implications including cancers have been traced to long-term arsenic intake,[5] and the WHO guideline imposes a stringent limit of 10 μg/L for arsenic in drinking water.[6]

Many chemical treatment options have been explored for arsenic removal, and these include coagulation, adsorption, ion exchange, and membrane processes.[7−11] Coagulation with alum or ferric chloride is commonly used in large-scale water treatment plants, and the process requires careful operation control.[7] Sorbents, such as activated carbon and metal oxides, or filtration units with an ion-exchange capability can be tailored for household or small community use, which offer a more practical solution in rural regions of the affected countries.[8−11] The principal forms of arsenic in the aqueous environments are arsenite (As(III), predominantly as H_3AsO_3) and arsenate (As(V), predominantly as $H_2AsO_4^-$ or $HAsO_4^{2-}$).[12,13] Amorphous or crystalline iron oxides possess strong affinity for both As(V) and As(III) species. Under neutral pH, both As(III) and As(V) adsorb strongly onto iron oxide surfaces via surface complex formation.[13,14] The molecular structures of arsenic−iron oxide complexes have been characterized by various spectroscopic techniques.[14−18]

Recent studies have shown that zerovalent iron (ZVI) is an effective remediation agent for treating arsenic-laden groundwater or drinking water.[19−23] It is generally conceived that As(III) and/or As(V) is removed by adsorbing on the iron oxide layer enclosing the ZVI particles[19,21] or forming coprecipitates with iron hydroxide produced during *in situ* iron corrosion.[20,23] However, spectroscopic investigations of

Received: September 6, 2011
Revised: February 8, 2012
Published: February 9, 2012

arsenic speciation in ZVI materials reveal that the immobilized arsenic is converted to different oxidation states from their aqueous forms, suggesting arsenic redox transformations play an active part in the remediation process. X-ray photoelectron spectroscopy (XPS) analysis by Su et al. detected partial oxidation of As(III) to As(V) by ZVI filing.[19] However, no reduction of As(III) was observed. Manning et al.[21] reported similar findings with X-ray absorption spectroscopy (XAS) for ZVI powders reacted under aerobic conditions, and they proposed the oxidation of As(III) might be mediated by iron corrosion products such as magnetite/maghemite or hematite. Bang et al.[22] found that a fraction of As(III) was reduced to As(0) on an acid-pretreated iron coupon under anoxic conditions. Because of variations in the experimental parameters and limited spectroscopic data sets published, a comprehensive understanding of the redox behavior is not yet available.

In recent years, attention has been focused on nanoscale zerovalent iron (nZVI) for its effectiveness in treating halogenated hydrocarbons, hexavalent chromium, and other heavy metal species in water.[24−26] The minute scale of the particles gives rise to an increased surface area, greater remediation capacity, and favorable field injection and transport properties for *in situ* remediation. While the nanoparticles have shown a remarkable efficacy to immobilize aqueous arsenic species,[27,28] the reactions involved appear to be more complex than those of iron oxides and the bulk-sized ZVI materials. Previous characterization of nZVI produced using a borohydride reduction method showed that the nanoparticles consist of a polycrystalline Fe(0) core encapsulated by a thin layer or shell of amorphous iron oxide averaging ∼3 nm in thickness.[29−31] The fine scale and defective nature of this oxide film may afford enhanced rates of electron transfer or mass diffusion across the oxide layer; thus, the nanoparticles may exhibit interesting redox behavior on a relatively small time scale that may not be manifested to an appreciable extent in the bulk iron counterparts. Indeed, we previously reported that arsenic in multiple valence states, including As(V), As(III), and As(0), were detected on nZVI particles reacted with aqueous As(III) species.[29] High resolution XPS (HR-XPS) multiline analysis indicates that these valence states are distributed in a layered structure with As(V) existing predominantly at the oxide surface, As(III) distributed across the oxide shell, and As(0) residing in a subsurface region close to the Fe(0) core.[30] These results demonstrate a dual redox capability of nZVI particles, whereby As(III) oxidation and reduction are enabled by the oxide shell and the Fe(0) core, respectively, resulting in preferential distributions of various arsenic valence states in different regions of the nanoparticles.

In this work, pertinent factors influencing the redox chemistry of nZVI and As(III) were investigated. Specifically, we compared arsenic speciation in reacted nZVI with those in iron oxides and a commercial micrometer-scale ZVI powder so as to understand the differences in arsenic removal mechanisms. Changes in arsenic valence states in the solid products with time and the long-term structural transformation of the arsenic-laden nanoparticles in the aqueous environment were evaluated. Findings from these analysis are to provide an improved reaction model between As(III) and nZVI.

EXPERIMENTAL METHODS

Preparation of Iron Materials. Iron nanoparticles (nZVI) were synthesized by reacting sodium borohydride ($NaBH_4$, 98% purity, Finnish Chemicals) with ferric chloride ($FeCl_3$, 98%, Alfa Aesar) following procedures reported previously.[31,32] The as-synthesized nZVI was stored in 95% ethanol solution in a sealed PTFE container at 4 °C prior to use. Two iron oxide powders, Fe_3O_4 and Fe_2O_3 (>99%, Fisher Chemical), were used in this study for comparison, whose reactions with As(III) have been extensively studied.[16,18,33] XRD characterization shows that the predominant mineral phases for Fe_3O_4 and Fe_2O_3 are magnetite and hematite, respectively. Additionally, a commercially available ZVI powder (H-200, Hoeganaes Corp.) with a median diameter of 85 μm was investigated. Prior to use, the ZVI powder was immersed in 0.5 N hydrochloric acid for 20 min to remove the surface passivation layer, followed by repeated rinsing with deionized water. The Brunauer−Emmet−Teller (BET) surface areas of nZVI, Fe_3O_4, and Fe_2O_3 were measured previously to be 29, 30, and 42 m^2/g, respectively,[30] and that of the micrometer-sized ZVI powder was 0.06 m^2/g.

Batch Experiments. As(III) and As(V) solutions were prepared from $NaAsO_2$ and $Na_2HAsO_4{\cdot}7H_2O$ (>98.5%, Fluka), respectively. Batch experiments of As(III) removal were performed in 120 mL serum bottles containing 100 mL of As(III) solution at 100 mg/L. The solution was deoxygenated by sparging with nitrogen (high purity, >99.9%) for 30 min immediately before the experiments. Upon adding an appropriate amount of iron material, the bottle was sealed with a screw cap lined with a Teflon-coated septum and placed on a mechanical shaker (250 rpm) at 25 °C. After a predetermined reaction time, a batch reactor was sacrificed, and the solids were separated from the solutions by vacuum filtration and dried for at least 12 h in a N_2 glovebox before transferring to XPS analysis chamber. The solution samples were stored in 40 mL glass vials at 4 °C and analyzed within 48 h of preparation. Details of aqueous sample analysis are available in the Supporting Information.

Microscopic Characterization. The structure and morphology of fresh and reacted nZVI were analyzed with a JEOL 2000FX TEM equipped with a LaB_6 source operating at 200 kV. The specimens were prepared by dispersing the N_2 dried solids in 95% ethanol, depositing a drop of this suspension on an amorphous carbon film supported on a 200 mesh copper grid, and allowing the sample to dry. The TEM was equipped with an energy dispersive X-ray spectrometer (EDS, Oxford Instruments) for X-ray point analysis. The spectra were collected from 0 to 20 keV at 20 eV/channel with a live time of 100 s.

HR-XPS Analysis. Dried samples of nZVI after reaction with As(III) were characterized using HR-XPS performed on a Scienta ESCA 300 spectrometer equipped with an 8 kW rotating anode source to provide monochromatic Al Kα ($h\nu$ = 1486.7 eV) radiation. Samples were analyzed in the C 1s, O 1s, As 2p, As 3d, and Fe 2p regions, which accounted for the major elements present at the surface. The effect of X-ray irradiation on samples was investigated by taking several short scans (∼40 s) on a sample during its exposure to X-ray irradiation for a period of time typical for routine analysis (10 min), and the results showed no measurable change in peak shapes and positions (Figure S1). In addition, the potential influence of visible light-induced photochemical reactions on our results can be excluded by specific experiments that showed no appreciable difference between the samples prepared in the dark and in normal room lighting conditions (Figure S2). More details on the HR-XPS analysis and curve-fitting of the spectra are provided in the Supporting Information.

dx.doi.org/10.1021/jp208600n | J. Phys. Chem. C 2012, 116, 5303−5311

RESULTS AND DISCUSSION

As(III) Removal from the Aqueous Phase. High efficacy of arsenic removal by nZVI at concentrations typical of its natural occurrence (10−1000 μg/L) has been noted in previous studies.[27,28] To directly examine arsenic reactions in the solid phase, higher concentrations are often needed to ensure adequate arsenic presence in the solids for accurate speciation analysis. For experiments presented herein, an initial As(III) concentration of 100 mg/L was used unless otherwise noted. As shown in Figure 1, over 99.9% of the As(III) in the solution was captured by 5 g/L of nZVI in 10 min. This rapid uptake of arsenic during the initial phase can be attributed to the formation of arsenic−iron coprecipitates in addition to adsorption. Formation of coprecipitates was conceivably promoted by rapid nZVI corrosion upon in contact with water releases a large amount of hydroxyl and dissolved iron species into the solution. This highly efficient removal process confirms that arsenic concentrations in the solid phase after 10 min of reaction were effectively constant. Therefore, the changes in arsenic valence states observed in subsequent XPS analysis were evidence of surface-mediated redox transformations instead of adsorption of reaction products formed in the solution phase.

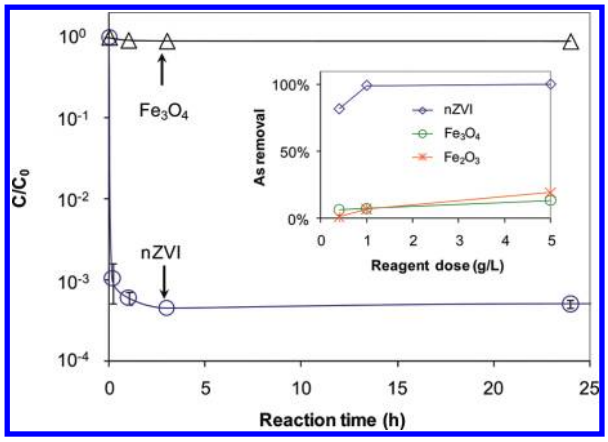

Figure 1. Change in aqueous arsenic concentration with time. Initial As(III) concentration (C_0) was 100 mg/L; nZVI or iron oxide dose was 5 g/L. Inset: percentage As(III) removal at various dose of iron materials after 24 h.

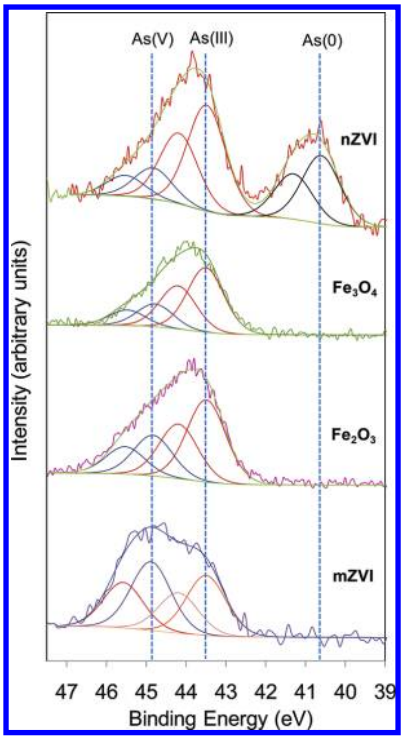

Figure 2. As 3d HR-XPS spectra of As(III) reacted with different iron or iron oxide materials. Initial As(III) concentration was 100 mg/L; mass loading of iron materials was 5 g/L; reaction time was 24 h.

In comparison, at an identical As(III) initial concentration and particle mass loading, Fe_3O_4 particles sequestered only 13% of the As(III) in the solution. A large difference in As(III) retention capacity between nZVI and the iron oxides can be clearly seen in the inset of Figure 1, which compares the final As(III) removal after 24 h by various doses (0.4−5 g/L) of nZVI, Fe_3O_4, and Fe_2O_3. Despite a relatively high initial concentration (100 mg/L), greater than 99% removal of As(III) was obtained with an nZVI dose as low as 1 g/L, whereas the removal efficiency remained below 20% even at the highest dose (5 g/L) of Fe_3O_4 and Fe_2O_3. Since the BET specific surface areas of nZVI and the two oxides are comparable (29−42 m^2/g), a direct comparison of mass-normalized As(III) removal capacity is possible. For nZVI, the maximum As(III) loading capacity is 2.2 mM As/g, while the value of the oxides is no more than 0.17 mM As/g. As a first-order estimate in which we consider that the average As(III) adsorption density on an iron oxide surface is ∼3 sites/nm^2,[2,13] one can estimate that the maximum As(III) uptake by the iron oxides is ∼0.2 mM As/g, which is consistent with the experimentally observed capacities. On the other hand, the capacity of arsenite removal by nZVI is well in excess of the total surface adsorption sites available, indicating that arsenite was not retained as merely a surface adsorbed layer.

Arsenic Speciation on the Solid Phase. HR-XPS spectra were acquired for the As 3d region on different iron materials reacted with As(III) for 24 h, and the results are shown in Figure 2. The binding energies (BE) of the different chemical states of the Ad3$d_{5/2}$ component were assigned as follows: As(V) 44.8 eV, As(III) 43.5 eV, and As(0) 40.6 eV.[29] The notation of As(0) does not necessarily imply it is in the elemental state. Rather, our independent analysis using X-ray absorption spectroscopy (XAS) suggests the reduced arsenic interacts with the Fe(0) environment forming an intermetallic-like structure. Since the exact valence state of this reduced arsenic is hard to define, we continue to denote it as As(0) here following the earlier studies.[29,30] It should be noted that if the distribution of species is not homogeneous across the sampling depth, the XPS technique is more sensitive to surface-residing species than those lying deeper due to increasing inelastic scattering of the photoelectrons with depth.[30,34] Therefore, the percentage values reported through XPS analysis are apparent concentrations only, assuming each species is distributed homogeneously throughout the depth. Despite this inherent assumption of XPS, the analysis is useful for comparing arsenic speciation across a sample set in which arsenic spatial distributions were similar.

As shown in Figure 2, the reacted nZVI contains As(V), As(III), and As(0) species at an apparent relative abundance of 14%, 51%, and 35%, respectively. The observation of As(V) and As(0) in the nZVI sample, which were not present in the initial solution, indicates that As(III) oxidation and reduction had taken place in the nanoparticles.[29] Our previous study

dx.doi.org/10.1021/jp208600n | J. Phys. Chem. C 2012, 116, 5303−5311

Table 1. Solution pH and E_h Values, Speciation of Solid-Phase Arsenic, and Aqueous Phase Arsenic and Iron Concentrations

					solid phase					solution	
iron material	As(III) initial conc (mg/L)	reaction time	final pH	final E_h (mV)	As(V)[a] (rel %)	As(III)[a] (rel %)	As(0)[a] (rel %)	As total[b] (at. %)	XPS spectrum	Fe (mg/L)	As[c] (C_{final}/C_0)
5 g/L nZVI	100	24 h	8.9	−49	14	51	35	1.36	Figs 2, 3, 6, 7	0.15	UD[d]
5 g/L Fe_3O_4	100	24 h	9.9	279	27	73	0	2.57	Fig 2	0.57	0.87
5 g/L Fe_2O_3	100	24 h	10.0	306	33	67	0	2.09	Fig 2	0.52	0.81
5 g/L mZVI	100	24 h	9.7	207	53	47	0	1.46	Fig 2	1.61	0.92
5 g/L nZVI	100	10 min			40	45	15	2.24	Fig 3	0.18	0.001
5 g/L nZVI	100	1 h	9.1	−44	23	51	26	1.50	Fig 3	0.23	UD[d]
5 g/L nZVI	100	15 days	8.7	−44	21	49	30	1.84	Fig 3	0.73	UD[d]
5 g/L nZVI	100	146 days	8.7	−180	11	45	44	1.80	Fig 3	0.28	UD[d]
5 g/L nZVI	10	24 h	8.5	−311	17	20	63	<1	Fig 6		
5 g/L nZVI	1	24 h	8.3	−310	19	42	39	<1	Fig 6		
0.4 g/L nZVI	100	24 h	9.5	199	45	55	0	3.60	Fig 7	1.84	0.82
1 g/L nZVI	100	24 h	9.9	157	27	73	0	5.32	Fig 7	0.17	0.04

[a]Determined by the relative intensities of individual arsenic valence state relative to that of total arsenic detected. [b]Determined by the intensity of As relative to those of other major species present, including C, Fe, and O, each normalized by the respective sensitivity factors. [c]Except for Figure 6, the initial As(III) concentration was 100 mg/L. [d]Final concentration below the detection limit (50 μg/L).

investigating the depth distribution of arsenic species in the near surface of nZVI by using different core levels (with their associated different probe depths) demonstrated that As(0) was predominantly located at the Fe(0)−core−oxide−shell interface, while the oxidized arsenic (As(V)) was present on the outer surface of the oxide in contact with the aqueous solution.[30] Thus, the oxidation and reduction processes were conceivably mediated by the oxide shell and the Fe(0) core, respectively.

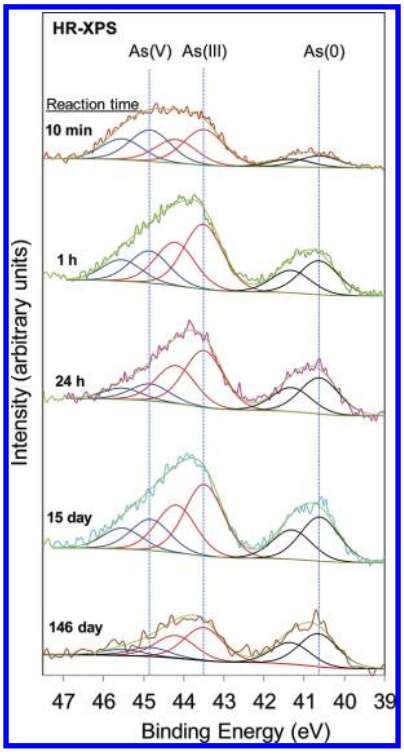

Figure 3. As 3d HR-XPS spectra of nZVI reacted with As(III) for different time. Initial As(III) concentration was 100 mg/L; nZVI loading was 5 g/L.

The As 3d spectra for the Fe_3O_4 and Fe_2O_3 samples indicate an apparent concentration of 27% and 33% of As(V), respectively. Previous studies reported that iron oxides, including magnetite, goethite (α-FeOOH), hematite (α-Fe_2O_3), and ferrihydrite, are able to induce As(III) oxidation in the presence of surface Fe(II) species.[33,35] The presence of Fe(II) species on the surfaces of the various iron materials can be inferred from the detection of an appreciable level of dissolved iron in the corresponding solution phase (Table 1). Fe(II) may come from aqueous corrosion of Fe(0), and in the case of iron oxides, it may present as a structural constituent or impurity. While several studies suggest that dissolved oxygen is required in addition to Fe(II) to produce reactive oxygen species (e.g., H_2O_2 or $OH^{\bullet}$ radical),[33,36] As(III) oxidation under anoxic conditions has also been reported, possibly occurring via a Fe(III) oxide−Fe(II)−As(III) surface ternary complex.[35] In the present study, the solutions were purged with pure nitrogen for 30 min (dissolved oxygen concentration measured after purging was ∼0.5 ppm), and anoxic conditions were maintained during experiments and sample drying. It is unlikely that the observed As(III) oxidation was caused entirely by reactive oxidants generated by the residue O_2, as this process can only oxidize ∼1% of the sequestered As(III) in the solutions. Additional mechanisms, e.g. oxidation of As(III) by the reactive Fe(II)−Fe(III) species on oxide surfaces,[35,37] may account for the observed data.

dx.doi.org/10.1021/jp208600n | J. Phys. Chem. C 2012, 116, 5303−5311

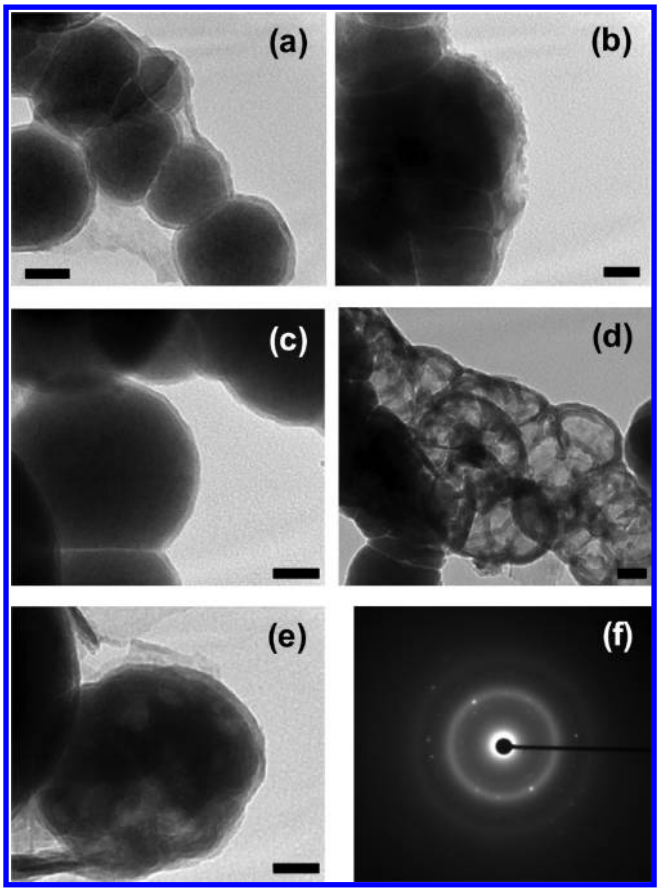

Figure 4. Bright-field TEM images of nZVI reacted with As(III) for (a, b) 24 h and (c–e) 146 days. Scale bar corresponds to 20 nm. (f) is the electron diffraction pattern of a particle shown in (c). The reactions were carried out with 5 g/L of nZVI and 100 mg/L of As(III).

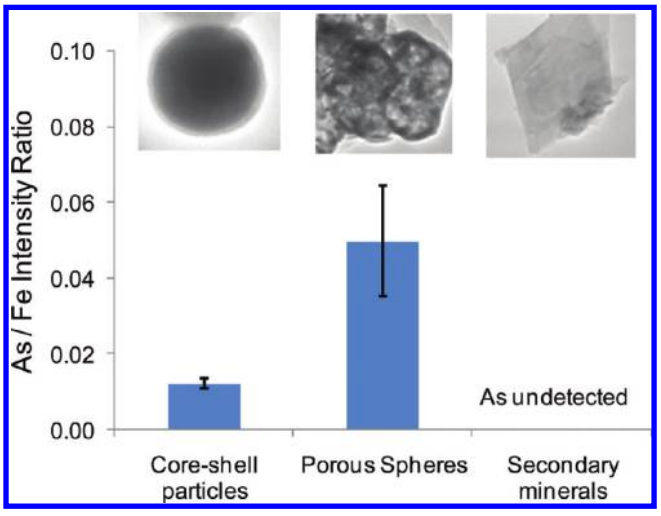

Figure 5. As Kα to Fe Kα peak intensity ratios of XEDS spectra obtained from three types of morphology found in the sample of nZVI reacted with As(III) for 146 days.

In contrast to nZVI, we did not detect As(III) reduction on a commercial micrometer-sized iron powder (denoted as "mZVI" in Figure 2), despite that the powder had been pretreated with hydrochloric acid to remove its surface passivation oxide.[22] Instead, the mZVI oxidized ~53% of As(III) to As(V). For this sample, a substantial amount of organic carbon containing

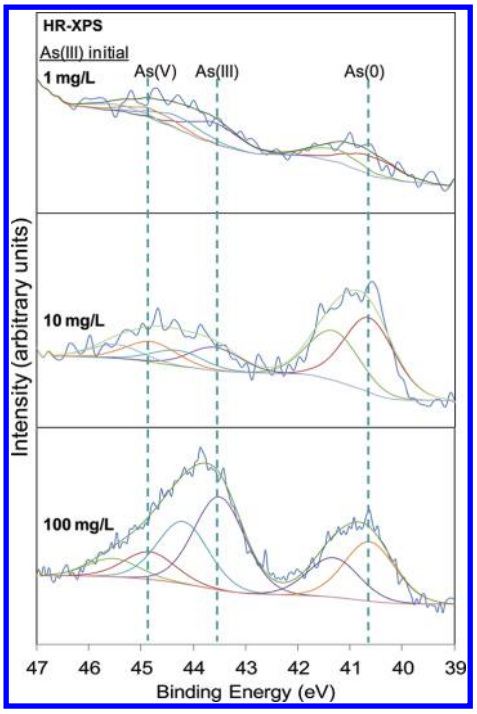

Figure 6. As 3d HR-XPS spectra of nZVI reacted with different initial concentrations of As(III). nZVI loading was 5 g/L; reaction time was 24 h. Intensity scale varies for each spectrum.

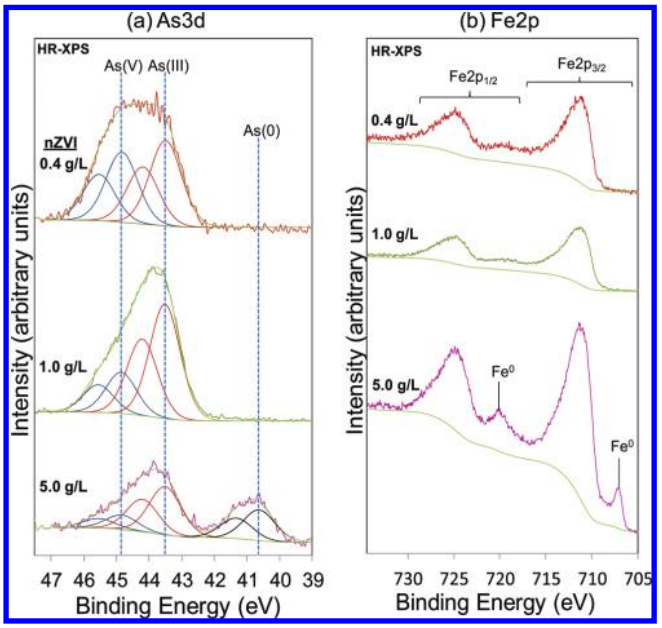

Figure 7. (a) As 3d and (b) Fe 2p HR-XPS spectra of varying dose of nZVI reacted with 100 mg/L As(III) for 24 h.

hydrocarbons (C–C), carboxyl (COO^-), and carbonyl (C=O) groups was detected on the particle surface, which could be residual grease or organic solvents used during the processing of the iron powder.[19] These impurities may contribute in part to the oxidation of As(III). Similar results including oxidation of As(III) to As(V) and the absence of reduced arsenic species have been noted by Su and Pul and Manning et al. with micrometer sized iron powders.[19,21] These results confirm that As(III) reduction is a unique capability of nZVI and constitutes an important sequestration mechanism.

dx.doi.org/10.1021/jp208600n | J. Phys. Chem. C 2012, 116, 5303–5311

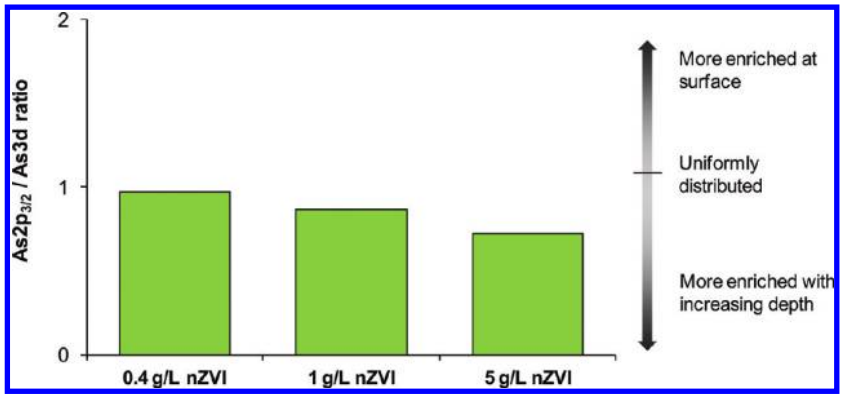

Figure 8. Intensity ratios of the As $2p_{3/2}$ and As 3d XPS spectra for the three samples in Figure 7. The procedure of obtaining these ratios from raw intensity data is mentioned in ref 30.

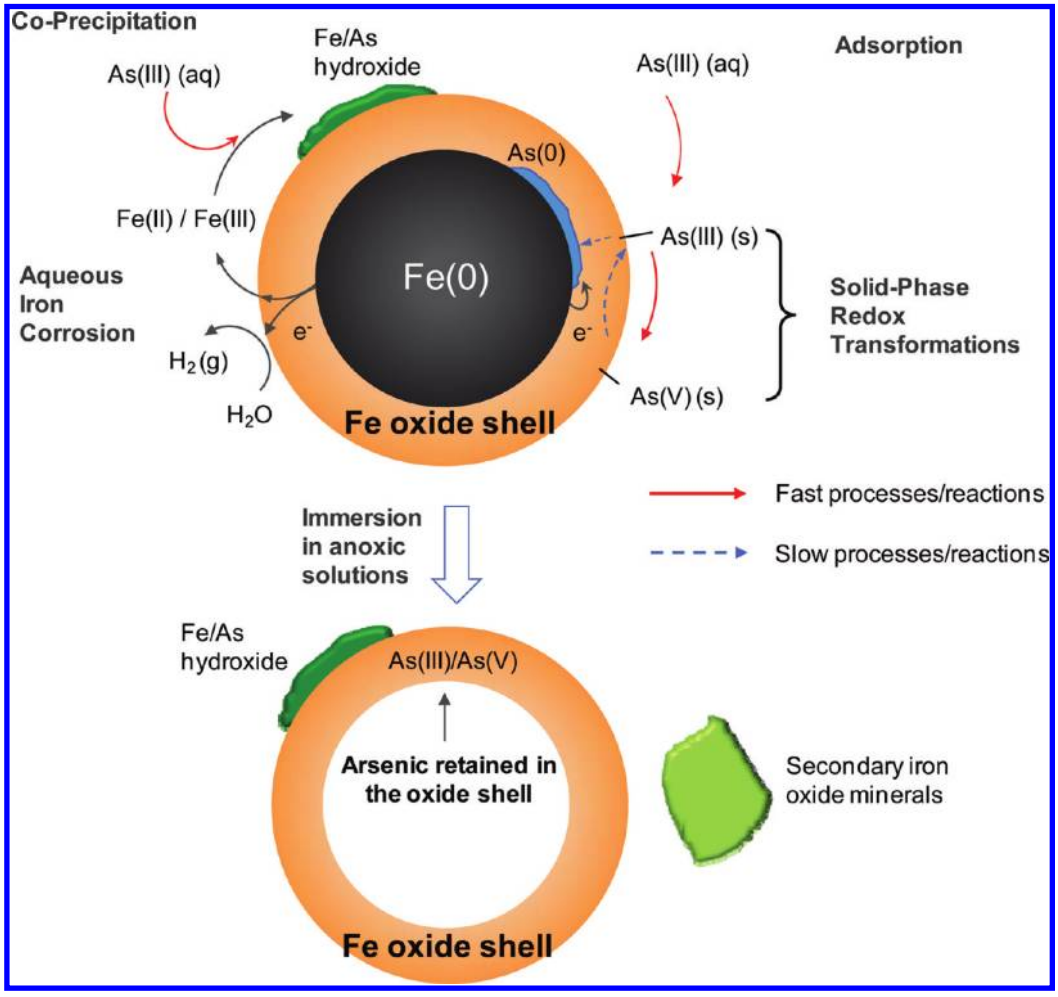

Figure 9. Schematic diagram summarizing processes responsible for arsenic removal in the As(III)−nZVI system in anoxic conditions. The relative scale of the core and shell components of nZVI is for illustration only and does not reflect actual dimensions. As(III) may be taken up from the aqueous phase by adsorption or coprecipitation. The solid-bound As(III) is oxidized rapidly at the oxide surface, while some As(III) diffuses and is reduced to As(0) near the oxide/Fe(0) interface. After prolonged immersion in an anoxic solution, the Fe(0) core is exhausted, leaving behind a vacant oxide shell with arsenic retained in the shell matrix.

Redox Transformation of Arsenic on nZVI over Time. The dynamic transformations of arsenic species on nZVI were investigated by analyzing the reaction products at various times between 10 min and 146 days. As shown in Figure 3, a significant amount of As(V) (~40% of the total arsenic) was observed at 10 min, indicating that As(III) oxidation is a fairly rapid reaction. The proportion of As(V) decreased gradually over the subsequent period of 146 days, suggesting the reverse reaction (As(V) → As(III)) took place at a much slower rate. Rapid As(III) oxidation has been reported in the presence of goethite and other mineral surfaces with adsorbed Fe(II) species.[35] This surface-mediated oxidation model is consistent with our prior finding that As(V) exists predominantly at the outer surface of the nanoparticles.[30] In contrast to the swift

dx.doi.org/10.1021/jp208600n | J. Phys. Chem. C 2012, 116, 5303−5311

oxidation of As(III), As(V) reduction to As(III) was much slower than the reverse reaction. Since As(V) reduction at the surface of a corroding ZVI media is unfavorable under neutral to alkaline pH,[38] the observed reduction may entail translocation of arsenic from the surface toward to the Fe(0) interface, and the kinetics is likely limited by the mass transport rate. Such inward migration of arsenic is in accordance with our previous analysis in which As(III) was observed to be present across the entire oxide layer.[30]

Further reduction of As(III) and progressive formation of As(0) were observed during the experimental period. As(0) constituted 15% of the total arsenic signal at 10 min and rose gradually to 35% after 24 h. This percentage did not change significantly afterward. After 146 days of aqueous immersion, 44% of the arsenic was reduced to As(0). This reduced form of arsenic was presumably located at a subsurface depth in adjacent to the Fe(0) core.[30] This ability of nZVI to induce movement of arsenic across the oxide shell is imparted by the core−shell nature of the nanoparticles. Prior studies show that the thin oxide film of iron nanoparticles is amorphous in nature.[29] It does not have a well-defined composition but exhibits a gradual transition from a mixed Fe(II)−Fe(III) oxide at the interface with Fe(0) to ferric oxyhydroxide at the outer periphery. The presence of oxygen vacancies and lattice disorder could give arise to elevated charge transfer and ionic mobility at room temperature.[41] Such properties can afford nZVI a distinctive redox reactivity and the ability to capture the contaminants in the interior of the particles, which were not observed in micrometer-sized iron powder and other conventional ZVI materials.[19−21,23]

Transformation of Arsenic-Laden nZVI over Time. The microstructure of as-synthesized nZVI has been characterized in previous studies.[26,31] Figures 4a,b show TEM images of nZVI that has reacted with an As(III) solution for 24 h. The core−shell structure remained largely unaltered during this reaction period. However, roughening of the oxide surface due to formation of granular deposits can be observed in the close-up image in Figure 4b. Figures 4c−e are particles that have undergone 146 days of reactions. Several types of distinctive morphology emerged in this sample. A fraction of the particles was devoid of the Fe(0) cores, leaving behind vacant shells of iron oxides (Figure 4d). Adjacent to these exhausted materials are particles that seem to have retained the original core−shell structure (Figure 4c). In between these two types of morphology is an intermediate structure as shown in Figure 4e, which holds tiny "bubbles" or cavities in the interior region. The coexistence of multiple structures shows that there is a significant variation in particle lifespan at the microscopic level. Factors such as the physical dimensions, grain size, crystallinity, and other structural attributes of the Fe(0) core and the oxide layer may influence the rate of iron oxidation. For those particles with metallic cores remain, the electron diffraction pattern of the core area contains sharp bright spot as shown in Figure 4f. This feature was absent for the as-synthesized particles,[29] and it demonstrates that the metal phase has undergone recrystallization during the period of 146 days. Similar observation has also been noted in a recent study on particle aging.[42] Coalescence and reformation of the Fe(0) grains may decrease the reactivity of the particles and preserve the iron content over a prolonged time.

To study the fate of the initially sequestered arsenic as the nanoparticles underwent continuous corrosion, X-ray fluorescence spectra were collected from the 146-day sample at regions corresponding to three types of morphology existing in this sample, viz., the core−shell particles, hollow spheres left upon depletion of the Fe(0) cores, and large angular platelets that are secondary minerals (e.g., ferrihydrite or goethite) formed as iron oxidation products.[27] For each type of morphology, three locations were analyzed, and the corresponding spectra are shown in Figure S3. Since direct elemental quantification is complicated by the overlapping O Kα and Fe Lα lines, we can use the ratio of As Kα to Fe Kα peak areas to indicate the relative amount of As in the solid residues. As shown in Figure 5, the ratio of As to Fe in the first type of morphology (core−shell particles) is 0.012 ± 0.0014, which is fairly consistent across three sampled locations. For the hollowed-out particles, arsenic was present at a much higher proportion (0.05 ± 0.015), whereas in the secondary oxide minerals, no arsenic was detected above the background. The absence of arsenic in the oxide minerals and in the final solution (Table 1) confirms that the sequestered arsenic did not leach out when the Fe(0) core was gradually consumed as a result of aqueous corrosion. The relatively large variation of arsenic levels in the hollow spheres suggests that these porous formations may include particles at different stages of oxidation. Those approaching complete exhaustion may exhibit higher ratios of As to Fe due to decreased Fe content within the structures.

Reactions at Lower Arsenic Concentrations. One limitation of XPS analysis is that a relative high concentration of arsenic has to be present in the solid phase in order to obtain unambiguous signals above the background noise. The lowest arsenic concentration used in previous studies was 50 mg/L,[29] which is still considerably higher than arsenic occurrence in the natural environment.[1,2] In this study, we attempted to analyze nZVI sample reacted with As(III) at 10 and 1 mg/L by increasing the X-ray irradiation time under optimized instrument conditions (detailed instrument settings available in the Supporting Information). The results are shown in Figure 6. It was noted in our previous studies that, as the initial concentration of As(III) decreased from 1000 to 50 mg/L, nZVI manifested a more reducing character due to less passivation caused by hydroxide precipitates formed at elevated As(III) concentrations. This trend is consistent with the behaviors shown in Figure 6, where reduction and the formation of As(0) account for approximately two-thirds of the total arsenic detected at the surface when the initial As(III) concentration was at 10 mg/L. At even lower As(III) concentration (1 mg/L), the spectrum is barely discernible above the background; thus, it is difficult to accurately assign the peak components via curve-fitting. We estimate that, in this sample, As(0) contributes to ∼40% of the total arsenic. It is noted from the figure that the relative percentage of As(V) is essentially invariant with respect to the initial As(III) concentration, implying arsenite oxidation is not strongly affected by the range of solution conditions studied here.

Effect of nZVI Dose. Figure 7a shows As 3d XPS spectra of samples reacted with As(III) solutions at different nZVI doses for 24 h. Notably, arsenic reduction was observed at the highest dose of nZVI (5 g/L), but not in 1 and 0.4 g/L samples. The corresponding Fe 2p XPS spectra in Figure 7b shows an Fe(0) component (707.0 eV) in the 5 g/L sample, which was absent at the lower doses of nZVI. The concomitant appearance of As(0) and Fe(0) corroborates with an earlier proposition that As(0) is embedded at the Fe(0)−oxide interface.[31] Since the XPS probe depth for Fe 2p photoelectrons is ∼6 nm,[34] the

dx.doi.org/10.1021/jp208600n | J. Phys. Chem. C 2012, 116, 5303−5311

absence of Fe(0) signals at 0.4 and 1 g/L nZVI suggests severe surface passivation or exhaustion of the Fe(0) cores. Similar findings can be made from the E_h values we measured in the solution phase (Table 1), which are much higher with smaller amounts of nZVI than that of the high-dose system. Extensive corrosion of the low-dose samples may well explain for the significant amounts of As(V) found in the final products (Figure 7a), since As(III) oxidation is promoted by the dissolved iron species generated from particle corrosion. Overall, with a small amount of nZVI, the Fe(0) cores play a diminishing role while the sequestered arsenic interact mainly with the oxide component. As such, we expect that arsenic is more uniformly incorporated in the oxide matrix as opposed to segregating as As(0) in the metal phase. This notion is indeed confirmed by the ratio of As $2p_{3/2}$ to As 3d XPS peak areas, which is an indicator of arsenic distribution within a near surface region of the sample (more details available in ref 31). As illustrated in Figure 8, at smaller doses of nZVI (0.4 and 1 g/L), the As $2p_{3/2}$ to As 3d ratios are close to one, implying arsenic was embedded fairly homogeneously in the oxide phase, thus accounting for the remarkable arsenic retention capacity observed in the solution experiments (inset of Figure 1).

Implications for As(III) Remediation. Previous studies of reactions between iron materials and arsenic focused chiefly on the adsorption and coprecipitation processes, the dynamic changes in arsenic valence states in nZVI reported here suggest redox reactions have occurred during nZVI treatment, and these reactions ultimately control the physical loci of different arsenic states in the particles. An improved reaction model incorporating the observed solid-phase redox transformations is depicted schematically in Figure 9. The different kinetics of these reactions and the continuous oxidation of nZVI in water caused the speciation of arsenic to change with time. This stresses the importance of viewing the arsenic−nZVI system as a dynamic rather than equilibrium-dominated system.

The results reported here have significant implications for the application of nZVI in arsenic remediation technologies. A distinct feature of nZVI relative to iron oxides and micrometer-sized ZVI powder is that the core−shell nature of the nanoparticles provides a considerable driving force for arsenic species to move into the interior of the nanoparticles or being captured in a growing oxide matrix instead of being retained as surface-bound species. This renders nZVI a potential good candidate for *in situ* applications in underground source zones and for use in centralized water treatment facilities.

Since nZVI is a reactive and consumable material, the stability of the sequestered arsenic over extended periods needs to be systematically evaluated. Although the present study shows that the sequestered arsenic remained in the solid matrix while Fe(0) was gradually depleted over a 5-month period, little is known about its eventual distribution and speciation under a wide range of geochemical conditions. Since microbial activity has a profound impact on iron redox reactions,[37,43] the transformations of nZVI and arsenic in natural or simulated microbiological environments will be of significant interest to the present field of study.

■ ASSOCIATED CONTENT

Supporting Information

Additional descriptions of the experimental and XPS curve-fitting procedures, pertinent properties of iron materials, surface elemental compositions by XPS analysis, and XEDS spectra of nZVI reacted for 146 days. This material is available free of charge via the Internet at http://pubs.acs.org.

■ AUTHOR INFORMATION

Corresponding Author

*Tel: 86-21-65982684; Fax: 86-21-65982693; e-mail zhangwx@tongji.edu.cn.

Present Address

⊥Civil and Environmental Engineering, Texas Tech University, Lubbock, TX 79409.

Notes

The authors declare no competing financial interest.

■ ACKNOWLEDGMENTS

This work was supported by a grant awarded to B.E.K. and W.Z. by the Pennsylvania Infrastructure Technology Alliance (PITA). B.E.K. acknowledges partial support of this work by the National Science Foundation under Grant 0616644.

■ REFERENCES

(1) Nordstrom, D. K. *Science* **2002**, *296*, 2143.
(2) Smedley, P. L.; Kinniburgh, D. G. *Appl. Geochem.* **2002**, *17*, 517.
(3) Meharg, A. A.; Rahman, M. *Environ. Sci. Technol.* **2003**, *37*, 229.
(4) Dittmar, J.; Voegelin, A.; Roberts, L. C.; Hug, S. J.; Saha, G. C.; Ali, M. A.; Badruzzaman, A. B. M.; Kretzschmar, R. *Environ. Sci. Technol.* **2010**, *44*, 2925.
(5) Mandal, B. K.; Suzuki, K. T. *Talanta* **2002**, *58*, 201.
(6) *WHO Guidelines for Drinking-Water Quality*, 3rd ed.; 2008; http://www.who.int/water_sanitation_health/dwq/gdwq3rev/en/index.html.
(7) Edwards, M. *J. Am. Water Works Assn.* **1994**, *86*, 64.
(8) Huang, C. P.; Vane, L. M. *J. Water Pollut. Con. Fed.* **1989**, *61*, 1596.
(9) Sarkar, S.; Gupta, A.; Biswas, R. K.; Deb, A. K.; Greenleaf, J. E.; SenGupta, A. K. *Water Res.* **2005**, *39*, 2196.
(10) Mohan, D.; Pittman, C. U. *J. Hazard. Mater.* **2007**, *142*, 1.
(11) Hussam, A.; Munir, A. K. M. *J. Environ. Sci. Health, Part A: Toxic/Hazard. Subst. Environ. Eng.* **2007**, *42*, 1869.
(12) Korte, N. E.; Fernando, Q. *Crit. Rev. Environ. Control* **1991**, *21*, 1.
(13) Dixit, S.; Hering, J. G. *Environ. Sci. Technol.* **2003**, *37*, 4182.
(14) Farquhar, M. L.; Charnock, J. M.; Livens, F. R.; Vaughen, D. J. *Environ. Sci. Technol.* **2002**, *36*, 1757.
(15) Manning, B. A.; Fendorf, S. E.; Goldberg, S. *Environ. Sci. Technol.* **1998**, *32*, 2383.
(16) Manceau, A. *Geochim. Cosmochim. Acta* **1995**, *59*, 3647.
(17) Goldberg, S.; Johnston, C. T. *J. Colloid Interface Sci.* **2001**, *234*, 204.
(18) Ona-Nguema, G.; Morin, G.; Juillot, F.; Calas, G.; Brown, G. E. *Environ. Sci. Technol.* **2005**, *39*, 9147.
(19) Su, C. M.; Puls, R. W. *Environ. Sci. Technol.* **2001**, *35*, 1487.
(20) Lackovic, J. A.; Nikolaidis, N. P.; Dobbs, G. M. *Environ. Eng. Sci.* **2000**, *17*, 29.
(21) Manning, B. A.; Hunt, M. L.; Amrhein, C.; Yarmoff, J. A. *Environ. Sci. Technol.* **2002**, *36*, 5455.
(22) Bang, S.; Johnson, M. D.; Korfiatis, G. P.; Meng, X. G. *Water Res.* **2005**, *39*, 763.
(23) Lien, H. L.; Wilkin, R. T. *Chemosphere* **2005**, *59*, 377.
(24) Ponder, S. M.; Darab, J. G.; Mallouk, T. E. *Environ. Sci. Technol.* **2000**, *34*, 2564.
(25) Liu, Y. Q.; Choi, H.; Dionysiou, D.; Lowry, G. V. *Chem. Mater.* **2005**, *17*, 5315.
(26) Li, X. Q.; Zhang, W. X. *J. Phys. Chem. C* **2007**, *111*, 6939.
(27) Kanel, S. R.; Manning, B.; Charlet, L.; Choi, H. *Environ. Sci. Technol.* **2005**, *39*, 1291.

(28) Kanel, S. R.; Greneche, J. M.; Choi, H. *Environ. Sci. Technol.* **2006**, *40*, 2045.
(29) Ramos, M. A. V.; Yan, W.; Li, X. Q.; Koel, B. E.; Zhang, W. X. *J. Phys. Chem. C* **2009**, *113*, 14591.
(30) Yan, W. L.; Ramos, M. A. V.; Koel, B. E.; Zhang, W. X. *Chem. Commun.* **2010**, *46*, 6995.
(31) Martin, J. E.; Herzing, A. A.; Yan, W. L.; Li, X. Q.; Koel, B. E.; Kiely, C. J.; Zhang, W. X. *Langmuir* **2008**, *24*, 4329.
(32) Sun, Y. P.; Li, X. Q.; Cao, J. S.; Zhang, W. X.; Wang, H. P. *Adv. Colloid Interface Sci.* **2006**, *120*, 47.
(33) Ona-Nguema, G.; Morin, G.; Wang, Y. H.; Foster, A. L.; Juillot, F.; Galas, G.; Brown, G. E. *Environ. Sci. Technol.* **2010**, *44*, 5416.
(34) Briggs, D., Seah, M. P., Eds.; *Practical Surface Analysis*; John Wiley & Sons: New York, 1990; Vol. *1*.
(35) Amstaetter, K.; Borch, T.; Larese-Casanova, P.; Kappler, A. *Environ. Sci. Technol.* **2010**, *44*, 102.
(36) Katsoyiannis, I. A.; Ruettimann, T.; Hug, S. J. *Environ. Sci. Technol.* **2008**, *42*, 7424.
(37) Borch, T.; Kretzschmar, R.; Kappler, A.; Van Cappellen, P.; Ginder-Vogel, M.; Voegelin, A.; Campbell, K. *Environ. Sci. Technol.* **2010**, *44*, 15.
(38) Melitas, N.; Conklin, M.; Farrell, J. *Environ. Sci. Technol.* **2002**, *36*, 3188.
(39) Wang, C. M.; Baer, D. R.; Amonette, J. E.; Engelhard, M. H.; Antony, J.; Qiang, Y. *J. Am. Chem. Soc.* **2009**, *131*, 8824.
(40) Signorini, L.; Pasquini, L.; Savini, L.; Carboni, R.; Boscherini, F.; Bonetti, E.; Giglia, A.; Pedio, M.; Mahne, N.; Nannarone, S. *Phys. Rev. B* **2003**, *68*, 195423.
(41) Kerisit, S.; Rosso, K. M. *J. Chem. Phys.* **2005**, *123*, 224712.
(42) Wang, Q.; Lee, S.; Choi, H. *J. Phys. Chem. C* **2010**, *114*, 2027.
(43) Tufano, K. J.; Fendorf, S. *Environ. Sci. Technol.* **2008**, *42*, 4777.